J|A|C|S
ARTICLES
Published on Web 08/10/2006

A Nanoengineering Approach to Regulate the Lateral Heterogeneity of Self-Assembled Monolayers

Jing-jiang Yu,[†] Yih Horng Tan,[†] Xue Li,[†] Pao-Kuang Kuo,[‡] and Gang-yu Liu*,[†]

Contribution from the Department of Chemistry, University of California, Davis, California 95616, and Department of Physics and Astronomy, Wayne State University, Detroit, Michigan 48202

Received May 4, 2006; E-mail: liu@chem.ucdavis.edu

Abstract: Using a scanning probe lithography method known as nanografting in conjunction with knowledge of self-assembly chemistry, regulation of the heterogeneity of self-assembled monolayers (SAMs) is demonstrated. While nanografting in single-component thiols produces areas of SAMs with designed geometry and size, nanofabrication in mixed thiol solution yields segregated domains. The reaction mechanism in nanografting differs significantly from self-assembly in mix-and-grow methods, as proven in systematic studies reported in this article and a companion paper of theoretical calculations of the nanografting process. Knowledge of the reaction pathways enables development of methods for shifting the interplay between the kinetics and thermodynamics in SAM formation, and thus the heterogeneity of mixed SAMs. By varying fabrication parameters, such as shaving speed, and reaction conditions, such as concentration and ratio of the components, the lateral heterogeneity can be adjusted ranging from near molecular mixing to segregated domains of several to tens of nanometers.

Introduction

Mixed self-assembled monolayers (SAMs) of organothiols on noble metal surfaces such as gold have attracted much attention because of their rich domain structures and variety of surface functionalities.[1,2] Additionally, mixed SAMs serve as better model systems than pure SAMs in mimicking biomembranes because of the presence of segregated domains.[3−9] Furthermore, mixed SAMs provide a powerful platform due to their rich structures and chemical and biological properties. For example, mixed SAMs have been employed for the study of a wide range of interfacial phenomena, such as wetting, electron transfer, and biomolecular adsorption and recognition.[10−15] Previous studies have revealed that the physical properties of binary SAMs such as the wettability,[10] friction,[16] and local elastic compliance[17] depend on the lateral heterogeneity or segregation of domains at the nanometer scale. Similarly, the chemical and biological properties vary with the local heterogeneity of the mixed SAMs. For example, stronger immobilization of enzyme molecules[18] and enhanced adsorption of DNA on surfaces[19] were realized by using a binary SAM containing the specific ligand with optimized surface composition. Cell adhesion and cellular functions such as motility can be affected by the distribution and arrangement of the receptor RGD domains on surfaces at the nanometer scale.[20] Therefore, finding an effective means to control or to regulate the lateral heterogeneity of mixed SAMs at the nanometer scale is critical in order to attain designed properties. The investigation of local domain structures should also facilitate an understanding of the self-assembly process and formation of membrane rafts.[21−23]

The formation of segregated domains in mixed SAMs results from the interplay between the reaction kinetics and thermo-

[†] University of California.
[‡] Wayne State University.

(1) Bain, C. D.; Evall, J.; Whitesides, G. M. *J. Am. Chem. Soc.* **1989**, *111*, 7155−7164.
(2) Bain, C. D.; Whitesides, G. M. *J. Am. Chem. Soc.* **1989**, *111*, 7164−7175.
(3) Stranick, S. J.; Atre, S. V.; Parikh, A. N.; Wood, M. C.; Allara, D. L.; Winograd, N.; Weiss, P. S. *Nanotechnology* **1996**, *7*, 438−442.
(4) Hobara, D.; Ota, M.; Imabayashi, S.; Niki, K.; Kakiuchi, T. *J. Electroanal. Chem.* **1998**, *444*, 113−119.
(5) Hobara, D.; Ueda, K.; Imabayashi, S.; Yamamoto, M.; Kakiuchi, T. *Electrochemistry* **1999**, *67*, 1218−1220.
(6) Kakiuchi, T.; Sato, K.; Iida, M.; Hobara, D.; Imabayashi, S.; Niki, K. *Langmuir* **2000**, *16*, 7238−7244.
(7) Chen, S. F.; Li, L. Y.; Boozer, C. L.; Jiang, S. Y. *J. Phys. Chem. B* **2001**, *105*, 2975−2980.
(8) Sawaguchi, T.; Sato, Y.; Mizutani, F. *J. Electroanal. Chem.* **2001**, *496*, 50−60.
(9) Klein, H.; Battaglini, N.; Bellini, B.; Dumas, P. *Mater. Sci. Eng., C* **2002**, *19*, 279−283.
(10) Imabayashi, S.; Gon, N.; Sasaki, T.; Hobara, D.; Kakiuchi, T. *Langmuir* **1998**, *14*, 2348−2351.
(11) Choi, S. H.; Lee, J. W.; Sim, S. J. *Biosens. Bioelectron.* **2005**, *21*, 378−383.
(12) Frederix, F.; Bonroy, K.; Laureyn, W.; Reekmans, G.; Campitelli, A.; Dehaen, W.; Maes, G. *Langmuir* **2003**, *19*, 4351−4357.
(13) Shen, G. Y.; Wang, H.; Tan, S. Z.; Li, J. S.; Shen, G. L.; Yu, R. Q. *Anal. Chim. Acta* **2005**, *540*, 279−284.
(14) Fan, F. R. F.; Yao, Y. X.; Cai, L. T.; Cheng, L.; Tour, J. M.; Bard, A. J. *J. Am. Chem. Soc.* **2004**, *126*, 4035−4042.
(15) Wakamatsu, S.; Akiba, U.; Fujihira, M. *Colloids Surf., A* **2002**, *198*, 785−790.
(16) Li, L. Y.; Chen, S. F.; Jiang, S. Y. *Langmuir* **2003**, *19*, 666−671.
(17) Price, W. J.; Kuo, P. K.; Lee, T. R.; Colorado, R.; Ying, Z. C.; Liu, G. Y. *Langmuir* **2005**, *21*, 8422−8428.
(18) Lahiri, J.; Isaacs, L.; Grzybowski, B.; Carbeck, J. D.; Whitesides, G. M. *Langmuir* **1999**, *15*, 7186−7198.
(19) Higashi, N.; Takahashi, M.; Niwa, M. *Langmuir* **1999**, *15*, 111−115.
(20) Maheshwari, G.; Brown, G.; Lauffenburger, D. A.; Wells, A.; Griffith, L. G. *J. Cell Sci.* **2000**, *113*, 1677−1686.
(21) Gregory, B. W.; Dluhy, R. A.; Bottomley, L. A. *J. Phys. Chem.* **1994**, *98*, 1010−1021.
(22) Fivaz, M.; Abrami, L.; van der Goot, F. G. *Protoplasma* **2000**, *212*, 8−14.
(23) Houseman, B. T.; Mrksich, M. In *Host-Guest Chemistry*; Springer−Verlag: Berlin, 2002; Vol. 218, pp 1−44.

10.1021/ja0631403 CCC: $33.50

dynamics. Much effort has been invested in investigating the impact of surface reaction conditions on the local domain structures.[6,8,24−30] Kinetics-driven products, i.e. mixed SAMs with a near molecular level mixing, were demonstrated during coadsorption of high concentration thiol mixtures (1 mM, C_{14}/C_8 = 7:1) at 50 °C.[24] Thermodynamics-driven layers, i.e., large segregated domains, were often observed after long immersion in dilute solutions and/or when the adsorbates' chain length and termini differ sufficiently, e.g. in mixed 3-mercapto-1-propanol and 1-tetradecanethiol (C_3OH/C_{14} = 1:1) at 1 μM thiol concentration.[30] In addition to the mix-and-grow approach referred to hereafter as natural self-assembly, the production of nanostructures with designed functionality, geometry, and dimensions can be achieved using nanolithography with single-component thiols, such as in nanografting[31−35] and DPN.[36,37] At larger dimensions, such as several to hundreds of micrometers or larger, structures can be produced using microlithography methods such as microcontact printing.[38,39]

In this article, we report a new approach of using nanografting in *mixed* thiols to regulate the local domain structure in mixed SAMs, ranging from molecular level mixing to nanometer islands. Regulation at the molecular and nanometer scale is attained by adjusting the interplay of self-assembly reaction kinetics and thermodynamics. A systematic investigation is presented using atomic force microscopy (AFM) imaging, nanolithography, and Monte Carlo simulation (see companion paper by Ryu and Schatz)[40] to reveal the complex reaction mechanisms of self-assembly of mixed thiols in natural growth as well in nanografting. A summary of our models for two self-assembly pathways are schematically shown in Figure 1. In natural growth (Figure 1A), thiol molecules collide with the gold surface via planar diffusion (see arrows), forming a stable reaction intermediate known as the "lying-down" phase. Continuous collision by thiols from solution builds up lateral pressure, which leads to a first-order phase transition where molecules stand up. Eventually monolayer coverage is reached with segregated domains locked in. This mechanism was established on the basis of investigations of single-component self-assembly using scanning probe microscopy.[41,42] In nanografting (Figure 1B) where the exposed gold area is less than the molecular chain length of alkanethiols, the adsorption follows a spatially confined self-assembly (SCSA) pathway. Thiol molecules within the matrix SAM are removed mechanically from the gold surface by a sharp AFM tip under high force. The freshly exposed area on the gold surface is small; as a result further deposition involves semispherical diffusion (see arrows in Figure 1B). The surface is also spatially confined by both the AFM tip and the neighboring thiol molecules in the matrix; thus, incoming thiols directly stand up, bypassing the lying-down to standing-up phase transition.[41,43] This pathway lowers the activation barrier and therefore exhibits kinetics at least 1 order of magnitude faster than that observed for the natural growth process.[43] In the actual nanografting process, both pathways occur, depending upon the transient spatial confinement conditions during nanofabrication. Therefore, our approach is designed to regulate the percentage at which SCSA occurs and, as a result, to impact the local structure of SAMs.

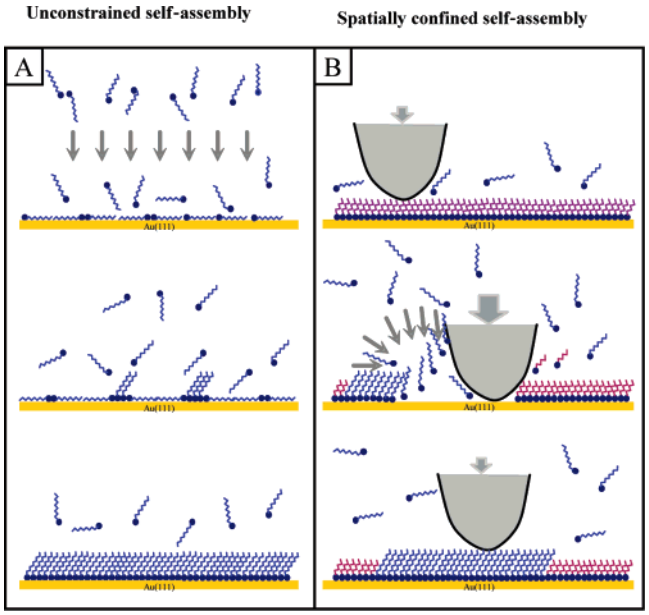

Figure 1. Schematic diagram illustrating the two surface reaction pathways of thiol self-assembly on gold: [A] unconstrained thiol adsorption occurs during natural self-assembly; and [B] spatially confined self-assembly (SCSA) occurs frequently in nanografting.

Experimental Section

Materials. *n*-Alkanethiols such as hexanethiol, decanethiol, dodecanethiol, and octadecanethiol (hereafter referred to as C_6, C_{10}, C_{12}, and C_{18}) and 3-mercaptopropionic acid (referred to as C_2COOH) with a purity of more than 95% were purchased from Aldrich and used without further purification. Aldehyde-terminated disulfide [$-S(CH_2)_{10}CHO]_2$ (referred to as $C_{10}CHO$ due to the cleavage of the disulfide bond [44]) was purchased from ProChimia (Gdansk, Poland). *sec*-Butyl alcohol was purchased from Fisher Scientific and used as the solvent for the mixed alkanethiol solutions without further purification.

Preparation of Binary Self-Assembled Monolayers (SAMs). Gold (Alfa Aesar, 99.999%) was deposited in a high-vacuum evaporator (Denton Vacuum, model DV502-A) at a base pressure below 2×10^{-6} Torr onto freshly cleaved mica substrates (clear ruby muscovite, Mica New York Corp.). The mica was preheated to 350 °C before deposition

(24) Chen, S. F.; Li, L. Y.; Boozer, C. L.; Jiang, S. Y. *Langmuir* **2000**, *16*, 9287−9293.
(25) Imabayashi, S.; Hobara, D.; Kakiuchi, T.; Knoll, W. *Langmuir* **1997**, *13*, 4502−4504.
(26) Hobara, D.; Sasaki, T.; Imabayashi, S.; Kakiuchi, T. *Langmuir* **1999**, *15*, 5073−5078.
(27) Shimazu, K.; Kawaguchi, T.; Isomura, T. *J. Am. Chem. Soc.* **2002**, *124*, 652−661.
(28) Arakawa, T.; Hobara, D.; Yamamoto, M.; Kakiuchi, T. *Electrochem. Commun.* **2005**, *7*, 848−852.
(29) Li, L. Y.; Chen, S. F.; Jiang, S. Y. *Langmuir* **2003**, *19*, 3266−3271.
(30) Hobara, D.; Kakiuchi, T. *Electrochem. Commun.* **2001**, *3*, 154−157.
(31) Xu, S.; Liu, G. Y. *Langmuir* **1997**, *13*, 127−129.
(32) Xu, S.; Miller, S.; Laibinis, P. E.; Liu, G. Y. *Langmuir* **1999**, *15*, 7244−7251.
(33) Xu, S.; Liu, G. Y. *Scanning* **1999**, *21*, 71−71.
(34) Headrick, J. E.; Armstrong, M.; Cratty, J.; Hammond, S.; Sheriff, B. A.; Berrie, C. L. *Langmuir* **2005**, *21*, 4117−4122.
(35) Schwartz, P. V. *Langmuir* **2001**, *17*, 5971−5977.
(36) Piner, R. D.; Zhu, J.; Xu, F.; Hong, S. H.; Mirkin, C. A. *Science* **1999**, *283*, 661−663.
(37) Salaita, K.; Amarnath, A.; Maspoch, D.; Higgins, T. B.; Mirkin, C. A. *J. Am. Chem. Soc.* **2005**, *127*, 11283−11287.
(38) Wilbur, J. L.; Kumar, A.; Kim, E.; Whitesides, G. M. *Adv. Mater.* **1994**, *6*, 600−604.
(39) Xia, Y.; Kim, E.; Whitesides, G. M. *J. Electrochem. Soc.* **1996**, *143*, 1070−1079.
(40) Ryu, S.; Schatz, G. C. *J. Am. Chem. Soc.* **2006**, *128*, 11563−11573.
(41) Poirier, G. E.; Pylant, E. D. *Science* **1996**, *272*, 1145−1148.
(42) Xu, S.; Cruchon-Dupeyrat, S. J. N.; Garno, J. C.; Liu, G. Y.; Jennings, G. K.; Yong, T. H.; Laibinis, P. E. *J. Chem. Phys.* **1998**, *108*, 5002−5012.
(43) Xu, S.; Laibinis, P. E.; Liu, G. Y. *J. Am. Chem. Soc.* **1998**, *120*, 9356−9361.
(44) Ishida, T.; Yamamoto, S.; Mizutani, W.; Motomatsu, M.; Tokumoto, H.; Hokari, H.; Azehara, H.; Fujihira, M. *Langmuir* **1997**, *13*, 3261−3265.

by using two quartz lamps which are mounted behind the mica to enhance the formation of terraced Au(111) domains. Typical evaporation rates were 3 Å/s, and the thickness of the gold films ranged from 1500 to 2000 Å. After the evaporation, the gold thin films were annealed at 365 °C under vacuum for 30 min and allowed to cool to room temperature. Immediately after removal from the chamber, the gold-coated substrates were annealed in a H_2 flame for 2 min in order to produce large terraces. Then, the gold films were quenched, either in pure ethanol or in air, to room temperature and immersed directly into the desired mixed alkanethiol solutions at least overnight before characterization by AFM and STM. This investigation focuses on mixed thiols of C_{18}/C_{10} where the functionality of both components is identical, and molecules differ only in chain length. To verify the robustness of our results, we also studied other types of mixed SAMs including C_{10}/C_6, C_{18}/C_{10}, $C_{10}CHO/C_6$, and C_{12}/C_2COOH. All SAMs are prepared and utilized within one week of the substrate immersion.

Atomic Force Microscopy. The AFM utilized was a home-constructed, deflection-type scanning head that exhibits high mechanical stability. The scanner was controlled by an AFM 100 preamplifier and STM 1000 electronic (RHK Technology, Inc. Troy, MI). The AFM scanner was calibrated laterally via the periodicity of a mica(0001) surface (0.518 nm) and vertically using the single atomic step of an Au(111) surface (0.235 nm). Sharpened Si_3N_4 microlevers (Veeco Metrology Group, Santa Barbara, CA) with a force constant of 0.1 N/m were used for AFM imaging. Images were acquired using contact mode in liquid media.

The optimal imaging area to visualize local domains is 100 nm × 100 nm under AFM. Both domain size (fwhm) and separation (center-to-center and edge-to-edge) were measured quantitatively from over 30 cursor profiles per image. The lateral heterogeneity is also analyzed using autocorrelation (RHK-based imaging processing software) and self-correlation (written using Mathematica). Self-correlation is defined as $G(k1,k2) = \sum f(x,y)\ f(x + k1, y + k2)$ where $f(x,y)$ represents the AFM topographic image. Typical tip diameter at the apex is 4 nm, estimated from imaging pure C_{18} vs C_{10} domains, and single atomic steps of Au(111),[45] and verified from blind-tip reconstruction (IgorPro-based AFM imaging and analysis software from Asylum Research). Image deconvolution was also performed and typically resulted in a less than 20% decrease of the lateral dimension of segregated domains. Given the accuracy of AFM and to maintain the integrity of the surface topograph, all images and analysis in this article are presented without tip-deconvolution processing.

Scanning Tunneling Microscopy. The STM used for this study incorporates a walker-type configuration scanner (UHV STM 300, RHK Technology, Inc. Troy, MI). The STM tips used for these studies are tungsten wires cut under ambient conditions and then electrochemically etched in 3 M KOH solutions at 2.1 V. A homemade electrochemical potentiostat was used to automatically monitor and stop the etching process when the current dropped below the setpoint. The STM scanner was calibrated laterally via the periodicity of decanethiol SAMs (periodicity 0.50 nm) and vertically using the single atomic step of an Au(111) surface. All images reported in this work were acquired in high-impedance, constant-current mode. The typical tunneling current was set at 30 pA and the bias voltage at 1 V.[46,47]

Nanografting. Nanografting is an AFM-based fabrication method developed in our group.[31−33] Briefly, a previously formed SAM serves as a matrix that is immersed in a solution containing the desired replacement thiol molecules. The matrix is imaged by the AFM tip under a low load. Once the fabrication location is chosen, the load is increased to above the displacement threshold of the adsorbed thiolated molecules. During the scanning, the matrix molecules are removed and replaced by thiols in solution as the AFM tip plows through the matrix monolayers.

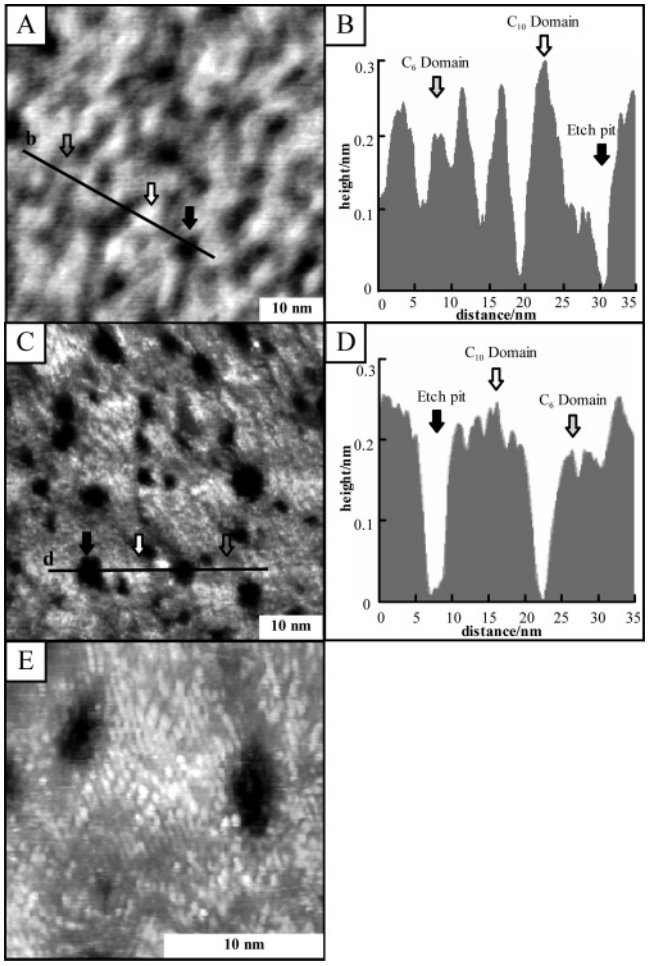

Figure 2. Molecular level characterization of the lateral heterogeneity of a binary C_{10}/C_6 SAM using AFM and STM imaging of the same system. The SAM is formed by natural growth from a mixed thiol solution with a total concentration of 0.02 mM and a molar ratio of C_{10}:C_6 = 1:5. [A] 50 nm × 50 nm AFM topographic image showing the local domain structures. [B] Cursor profile corresponding to the line in [A]. [C] 50 nm × 50 nm STM image revealing the local domain structures. [D] Cursor profile corresponding to the line in [C]. [E] 20 nm × 20 nm zoom-in scan by STM to show the molecular mixing within the C_{10} and C_6 domains.

Results and Discussion

High-Resolution Structural Characterization of SAMs from Mix-and-Grow. The local domains in naturally grown mixed SAMs can be clearly visualized using AFM, and molecular level resolution is attainable using STM.[8,24,48] We have initiated our investigation by characterizing the structures of binary C_{10}/C_6 SAMs to provide a structural base for comparison of mixed alkanethiol SAMs, and to validate our study with previous work.[6,8,9,24,48−50] Figure 2A is a 50 nm × 50 nm AFM topographic image of a binary C_{10}/C_6 SAM prepared by natural growth. This SAM clearly consists of domains as evidenced by the bright and gray contrasts. Etch

(45) Xu, S.; Amro, N. A.; Liu, G. Y. *Appl. Surf. Sci.* **2001**, *175*, 649−655.
(46) Qian, Y. L.; Yang, G. H.; Yu, J. J.; Jung, T. A.; Liu, G. Y. *Langmuir* **2003**, *19*, 6056−6065.
(47) Yang, G. H.; Qian, Y. L.; Engtrakul, C.; Sita, L. R.; Liu, G. Y. *J. Phys. Chem. B* **2000**, *104*, 9059−9062.
(48) Tamada, K.; Hara, M.; Sasabe, H.; Knoll, W. *Langmuir* **1997**, *13*, 1558−1566.
(49) Kakiuchi, T.; Iida, M.; Gon, N.; Hobara, D.; Imabayashi, S.; Niki, K. *Langmuir* **2001**, *17*, 1599−1603.
(50) Munakata, H.; Kuwabata, S.; Ohko, Y.; Yoneyama, H. *J. Electroanal. Chem.* **2001**, *496*, 29−36.

pits, 2−5 nm wide and with the depth of a single atomic step of Au(111), are clearly visible. The overall morphology and the size/distribution of etch pits are characteristic of freshly prepared SAMs from solution phase, according to previous diffraction and STM investigations of pure and mixed SAMs.[4,46,51,52]

The lateral dimensions of the domains are extracted from the cursor profiles as shown in Figure 2B; they range from 3 to 6 nm with an average separation of 8 nm. The height difference between the white and gray areas measures 0.15 nm, smaller than the predicted value of 0.44 nm using the 30° tilt angle[53−56] for thiols in SAMs. The imaging force is 1.6 nN; thus, the SAM deformation is less than 0.2 nm as estimated from the Hertzian model.[57−61] This deformation alone is insufficient to account for the observed height difference. Therefore, we conclude that the height difference is due to the fact that the white and gray regions are not pure C_{10} and C_6, respectively. Instead, white areas contain mixtures of both components with a greater number of C_{10} molecules; these areas are referred to as C_{10}-rich domains or C_{10} domains for short. This mixing disrupts the molecular level close-packing and thus permits higher deformation under AFM imaging pressure than for periodic SAMs, which leads to a smaller height difference than the theoretical value. This deviation from the theoretical value also provides a quantitative measure of the degree of mixing within domains.

Molecular level characterization of these local domains is attained using STM. Figure 2C is a STM topographic image with the same scan size as that of the AFM image in Figure 2A. The overall surface morphology including the features of etch pits is very similar to that revealed in AFM. The average size of C_{10} domains is 5.5 nm (ranging from 3.8 to 7.2 nm) from STM topographs, which is ∼16% smaller than that measured from AFM images (6.5 nm). This small discrepancy is likely due to AFM tip convolution. Given the variation of the domain size and the accuracy of the technique, the two methods provide very consistent measurement of local domain structures. Further zooming in, shown in Figure 2E, reveals that the bright areas contain 80% C_{10}, while the gray areas have less than 30% of the C_{10} thiol molecules. Since panels A and C of Figure 2 reveal very similar domain sizes and distribution, we use high-resolution AFM for most of the other mixed SAMs, bearing in mind the mixing within domains. Further, most thiols used in membrane-mimicking SAMs are longer than C_{10}, which are not sufficiently conductive for STM investigations. Various scanning sizes were used to reveal surface morphology as well as local domains. We observed that 100 nm × 100 nm scans are sufficiently small in the visualization of local domain structures. Our observation of the local structure is consistent with previous research on mixed SAMs, i.e., mixed thiols form separated domains on gold with the lateral heterogeneity varying with experimental conditions.[1−3,7,8,24,48]

Structural Differences in Local Domains: Nanografted versus Naturally Grown SAMs. As a direct result of the two self-assembly pathways (see the models shown in Figure 1), more kinetics-driven SAMs are formed in nanografting, while more thermodynamic-driven layers are formed in natural growth. Figure 3 provides unambiguous proof, in which areas of nanografted SAMs and natural grown layers were produced on the same gold surface from the same mixed thiol solution: a 2 μM thiol in 2-butanol with C_{18}/C_{10} = 3:5; further, both SAMs were characterized side-by-side under the same imaging conditions. Figure 3A reveals the overall morphology of the mixed SAM in an 800 nm × 800 nm area, within which a 400 nm × 400 nm region is produced by using nanografting. As the first observation, the boundaries of the nanografted area are clearly visible because the pattern is 0.45 nm lower (see Figure 3D) than the surrounding matrix. Following the discussion pertaining to Figure 2, this height difference suggests that nanografted SAMs exhibit a lower degree of domain segregation than the naturally grown ones. Second, the fabricated binary area appears smoother than that of the matrix SAM, as also evidenced by the better resolved Au(111) steps in the central grafted area than in the surrounding areas. Cursor profiles shown in E and F of Figure 3 indicate the surface roughness is 0.27 and 0.14 nm, respectively. The smaller surface roughness further supports the higher degree of molecular mixing in the nanografted SAMs. Finally, the lateral heterogeneity of local domains is visualized from high-resolution images shown in panels B and C of Figure 3. In a 100 nm × 100 nm scan, the segregated C_{18} and C_{10} domains and their spatial distribution are clearly visible. The nanografted SAMs exhibit smaller C_{18} domains that are less separated than those in the matrix counterpart. The quantitative heterogeneities of nanografted vs naturally grown SAMs, as measured by the size and separation of local domains as well as the height difference in surface morphology, have been extracted from cursor profiles and are summarized in Table 1. Compared to the naturally grown matrix in which the average C_{18} domain size and separation (center-to-center) are 7.5 and 17.9 nm, respectively, SAMs from nanografting exhibit a decrease in size and separation by ∼40%, i.e., they demonstrate less heterogeneity.

If the local structure of SAMs were purely determined by thermodynamics, the surface concentration would be C_{18}:C_{10} = 76:1 (see Supporting Information for detailed derivation based on surface reaction thermodynamics). In other words, 98.7% of Au(111) would be covered by C_{18} domains. In both nanografting and natural growth as shown in Figure 3, the actual C_{18} coverage and domain size fall significantly below the thermodynamic limit, which means the interplay favors kinetics under those experimental conditions. Further, the as-grown SAMs are closer to the thermodynamic structure than are the nanografted areas, i.e., they exhibit higher heterogeneity. The heterogeneity can also be quantified using the position self-correlation function, as shown in panels G and J of Figure 3 for both SAMs, respectively. The broader central and satellite peaks (see Figure 3, H and I, versus Figure 3, K and L) indicate a higher degree of segregation in natural growth than in

(51) Poirier, G. E. *Chem. Rev.* **1997**, *97*, 1117−1127.
(52) Poirier, G. E. *Langmuir* **1997**, *13*, 2019−2026.
(53) Nuzzo, R. G.; Allara, D. L. *J. Am. Chem. Soc.* **1983**, *105*, 4481−4483.
(54) Fenter, P.; Eisenberger, P.; Liang, K. S. *Phys. Rev. Lett.* **1993**, *70*, 2447−2450.
(55) Camillone, N.; Chidsey, C. E. D.; Liu, G. Y.; Scoles, G. *J. Chem. Phys.* **1993**, *98*, 3503−3511.
(56) Nuzzo, R. G.; Fusco, F. A.; Allara, D. L. *J. Am. Chem. Soc.* **1987**, *109*, 2358−2368.
(57) Hu, J.; Xiao, X. D.; Salmeron, M. *Appl. Phys. Lett.* **1995**, *67*, 476−478.
(58) Kiridena, W.; Jain, V.; Kuo, P. K.; Liu, G. Y. *Surf. Interface Anal.* **1997**, *25*, 383−389.
(59) Price, W. J.; Leigh, S. A.; Hsu, S. M.; Patten, T. E.; Liu, G. Y. *J. Phys. Chem. A* **2006**, *110*, 1382−1388.
(60) Carpick, R. W.; Ogletree, D. F.; Salmeron, M. *Appl. Phys. Lett.* **1997**, *70*, 1548−1550.
(61) Hues, S. M.; Draper, C. F.; Colton, R. J. *J.Vac. Sci. Technol., B* **1994**, *12*, 2211−2214.

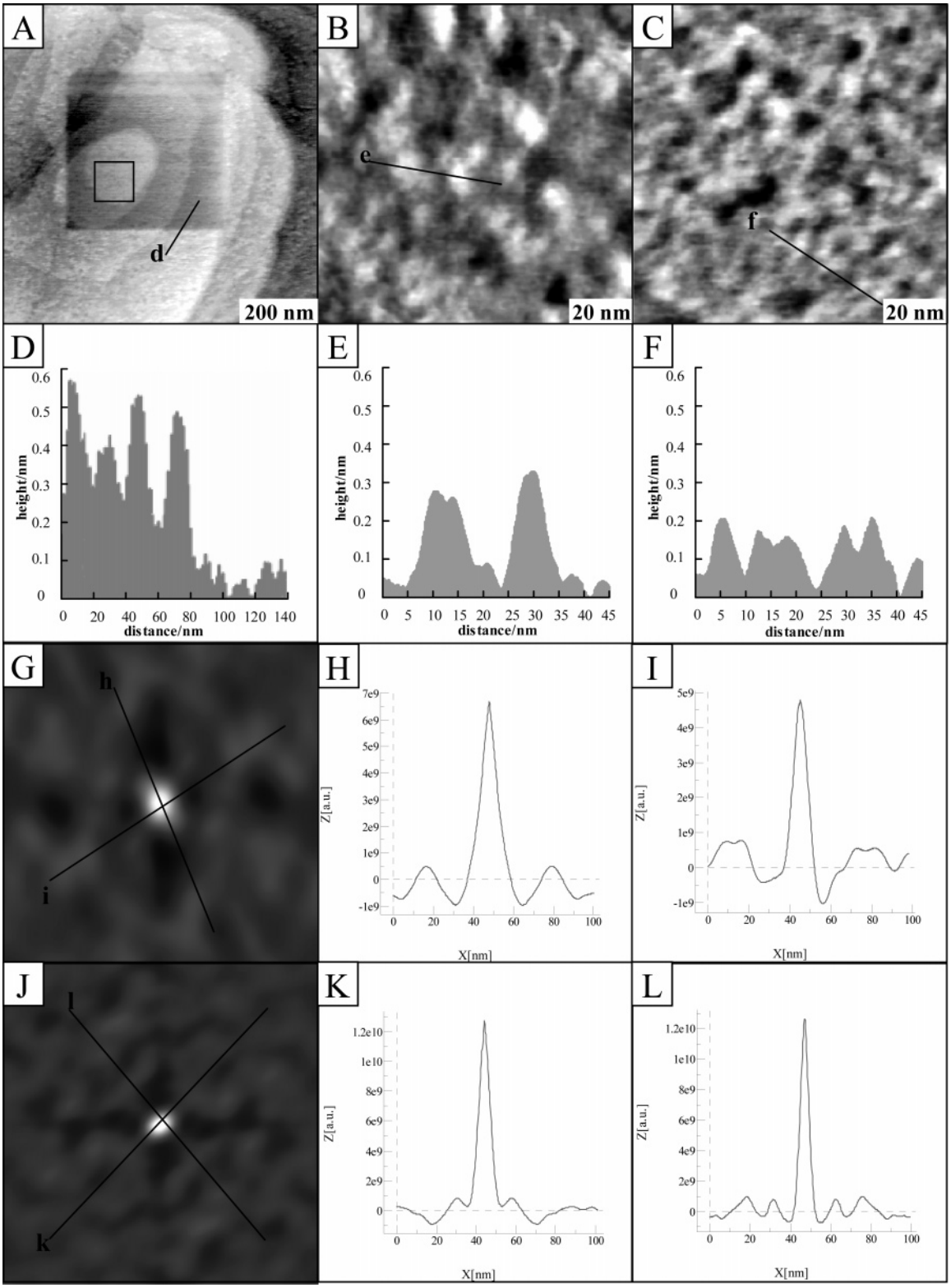

Figure 3. Comparison of local domain structures of mixed C_{18}/C_{10} SAMs formed with nanografting (fabrication speed = 500 nm/s) versus that with natural growth. SAMs are formed from the same thiol solution (0.002 mM with C_{18}:C_{10} = 3:5). [A] 400 nm × 400 nm AFM topograph reveals the overall morphology of SAMs produced by the two methods. [B] Zoom-in scan (100 nm × 100 nm) of the matrix SAM. [C] Zoom-in scan (100 nm × 100 nm) in the nanografted area as indicated in [A]. [D−F] Cursor profiles crossing the lines indicated in images [A−C], respectively. [G] Self-correlation of image [B] to reveal the lateral heterogeneity of the natural grown SAM. [H, I] Cursor profiles as indicated in [G]. [J] Self-correlation of image [C] to reveal the lateral heterogeneity of the nanografted SAM. [K, L] Cursor profiles as indicated in [J].

nanografting. The fact that nanografting did not completely reach molecular level mixing (C_{18}:C_{10} = 3:5) suggests that two pathways coexist in the nanofabrication process, depending on transient local confinement. This description of self-assembly and nanografting is further illustrated in the Monte Carlo simulations in the companion paper.[40]

Table 1. Comparison of the Lateral Heterogeneity of Mixed SAMs Prepared by Natural Self-assembly and Nanografting

mixed thiol solution	SAM preparation method	average domain size of long-chain thiols (nm)	average domain separation (nm)		height difference between bright and gray areas (nm)	
			center-center	edge-edge	theory	exp.
C_{18}/C_{10} (3:5, 0.002 mM)	natural growth	7.5	17.9	10.4	0.88	0.27
	nanografting	4.7	10.0	5.8		0.16
$C_{10}CHO/C_6$ (4:1, 0.1 mM)	natural growth	8.9	13.6	6.1	0.55	0.12
	nanografting	5.1	9.0	4.4		0.08
C_{12}/C_2COOH (1:10, 0.02 mM)	natural growth	9.3	18.1	9.1	0.79	0.20
	nanografting	6.8	10.9	4.9		0.13

The differences in local domains as a result of the two SAM preparation methods have also been observed for mixed SAMs with various functional termini, some of which are listed in Table 1. The level of component segregation in naturally grown SAMs may be enhanced, or the level of mixing is decreased, by mixing thiols with a large chain-length differences, or with different termini. Table 1 includes two other pairs from a variety of mixed SAMs we have tested, carboxylic acid and aldehyde-termini. Figure 4A shows a 450 nm × 450 nm AFM topograph of a binary $C_{10}CHO/C_6$ SAM with the central 200 nm × 200 nm nanografted region produced from the same mixed thiol solution. Panels B and C of Figure 4 are the zoom-in scans of the matrix and grafted areas, respectively. Similar to the mixed C_{18}/C_{10} system, the nanografted area of $C_{10}CHO/C_6$ exhibits lower heterogeneity than the surrounding as grown SAM.

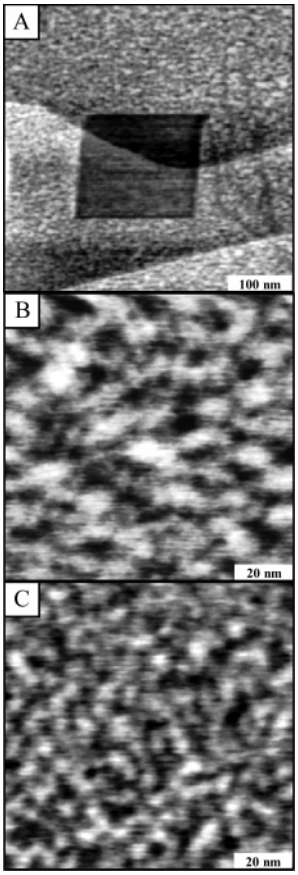

Figure 4. Comparison of local domain structures of mixed $C_{10}CHO/C_6$ SAMs formed with nanografting (fabrication speed = 1000 nm/s) versus that with natural growth. SAMs are formed from the same thiol solution (0.1 mM with $C_{10}CHO/C_6$ = 4:1). [A] 450 nm × 450 nm AFM topograph reveals the overall morphology of SAMs produced by the two methods. [B] Zoom-in scan (100 nm × 100 nm) of the matrix SAM. [C] Zoom-in scan (100 nm × 100 nm) in the nanografted area.

Due to the higher Gibbs energy difference between the two components, the $C_{10}CHO/C_6$ SAMs is more segregated than the C_{18}/C_{10} systems.

The trend toward component segregation for mixed SAMs is consistent with previous reports.[4,8,9,48,49] The level of segregation may be enhanced while the level of mixing is decreased by use of thiols with a large chain-length difference, or with different termini. The heterogeneity of mixed C_{18}/C_4 (octadecanethiol/butanethiol) SAMs as reported by Tamada et al.[48] is larger than that in our C_{10}/C_6 systems. Similar behavior was observed for binary C_2COOH/C_{10} SAMs.[8] The C_{10} domains exhibit a densely packed $(\sqrt{3}\times\sqrt{3})R30°$ structure that is consistent with the well-characterized structure of *n*-alkanethiol monolayers while a completely different molecular arrangement of C_2COOH defined as a (3 × 3) structure was consistently observed in the C_2COOH domains, implying that the composition of both C_{10} and C_2COOH domains may be or is close to completely single component.

Nanografting Enables a Wide Range of Regulation of the Lateral Heterogeneity of SAMs. We have discussed the self-assembly mechanism in constrained and unconstrained local environments using the models in Figure 1 as well as in the companion paper.[40] At any given location of nanofabrication, thiol self-assembly follows one specific pathway, depending upon the transient spatial constraint. While the precise determination of the local environment requires the knowledge of exact tip and molecular movements under shaving pressure, one can effectively impact the transient environment by varying the shaving speed. We have conducted a systematic speed-dependence experiment with three characteristic data points shown in Figure 5. At a shaving speed of 500 nm/s as shown in Figure 5A, nanografting in a mixed C_{18}/C_{10} solution (1:5 molar ratio with 0.02 mM concentration) resulted in a relatively homogeneous mixing of the two components. The average C_{18} domain size is 2.7 nm with a center-center spacing of 5.5 nm. Slow-shaving results in transient spatial constraint during fabrication; thus, thiols follow the SCSA pathway, i.e., diffusion and kinetics dictate the local domain structure of the SAM. Increasing the shaving speed decreases the transient spatial confinement; thus, one should anticipate that the natural-growth pathway would dominate at the locations where the exposed gold area is sufficiently large and not confined by the tip and surrounding thiols. An explanation for this is shown in the models in D and E of Figure 5. In fact, this trend is observed by comparing the SAMs grafted under 3,000 nm/s (Figure 5B) versus 500 nm/s (Figure 5A). At 3,000 nm/s, the average C_{18} domain size is increased to 5.5 nm with a center-to-center separation of 11.2 nm. Further increase of the fabrication speed to 10,000 nm/s leads to a SAM morphology as shown in Figure 5C, with an average C_{18} domain size of 8.9 nm and a 15.0 nm

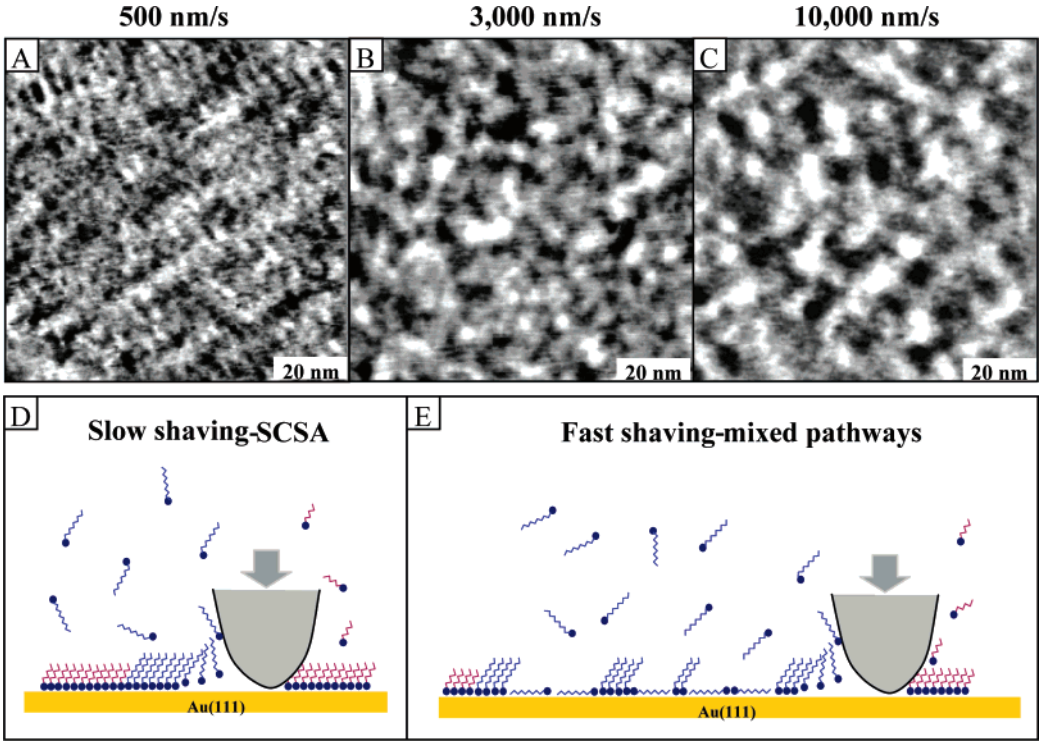

Figure 5. Regulation of the lateral heterogeneity of mixed SAMs by varying the shaving speeds in nanografting. Under the same binary thiol solution, 0.02 mM thiol in 2-butanol with $C_{18}/C_{10} = 1{:}5$, a series of nanografting scans were taken with increasing shaving speed from one image to the next. [A−C] Scans with three characteristic speeds 500, 3000, and 10000 nm/s, respectively. The total scan area for all images shown is 100 nm × 100 nm. [D, E] Schematic diagrams illustrating the proposed mechanism of SAM growth under the two methods.

separation, a product nearly the same as that produced via natural self-assembly. We note that the threshold of "slow" versus "fast" shaving speed varies, depending on the detailed tip−surface interactions, tip geometry, and surface reaction conditions. Therefore, the speed threshold at which SCSA occurs must be measured for each experiment. The trend of the speed dependence shown in Figure 5 is valid in all experiments performed and is also reflected in the Monte Carlo simulations.[40] Investigation of speed dependence demonstrates that under a given mixed thiol solution, nanografting enables the production of mixed SAMs with designed heterogeneity from molecular mixing to the component segregation of natural growth, by simply increasing shaving speed. This new approach of using nanografting offers the advantages of (a) simplicity, e.g. adjustment of only a single parameter (speed); (b) high throughput because one does not need to reprepare thiol solutions or repeat the entire procedure; and (c) full range of control from molecular level mixing to segregation at the nanometer scale.

At medium or fast shaving speed, the pathway of natural self-assembly is followed at locations where spatial confinement is not sufficient. Therefore, we anticipate that surface reaction conditions that impact natural self-assembly would similarly influence the results of nanografting. Figure 6 reveals the influence of overall thiol concentration. The concentration dependence of natural self-assembly is shown in the left column of Figure 6 as a comparison. In the case of natural self-assembly, SAMs formed from a 0.2 mM thiol solution (C_{18}:C_{10} = 1:1) exhibit an average C_{18} domain size of 4.9 nm with 8.9 nm separation. Decreasing the overall concentration while maintaining the ratio resulted in an increase of C_{18} domain size to 8.2 and 11.1 nm, at 0.02 and 0.002 mM, respectively. The increase in heterogeneity with the decrease of thiol concentration is

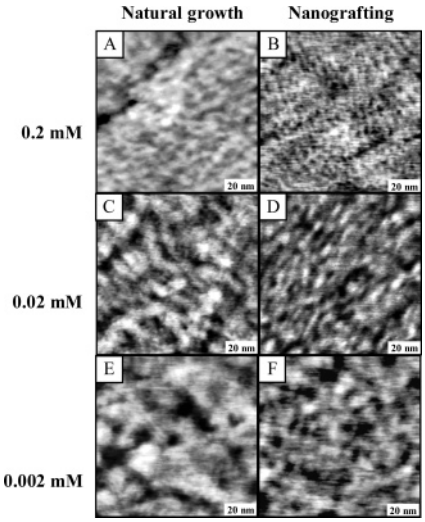

Figure 6. Regulation of the lateral heterogeneity of mixed SAMs by varying the overall concentration of thiols, natural self-assembly (left column) versus nanografting (right column). Under the same imaging and nanografting conditions (500 nm/s shaving speed), three sets of SAMs were prepared with decreasing thiol concentrations as indicated. SAMs within each row were prepared under the same thiol solution where the $C_{18}/C_{10} = 1{:}1$ so that the results from the two methods can be directly compared. The decrease in thiol concentration resulted in more thermodynamically favored products, i.e., larger domains; the impact of concentration is stronger in natural self-assembly than in nanografting.

consistent with known observations[30] and with the prediction that low concentration favors thermodynamic products. This observation is also analogous to crystal growth, where lower concentration leads to larger-sized single crystals. The right column in Figure 6 shows the corresponding nanografting experiments, where a similar trend was also observed. The

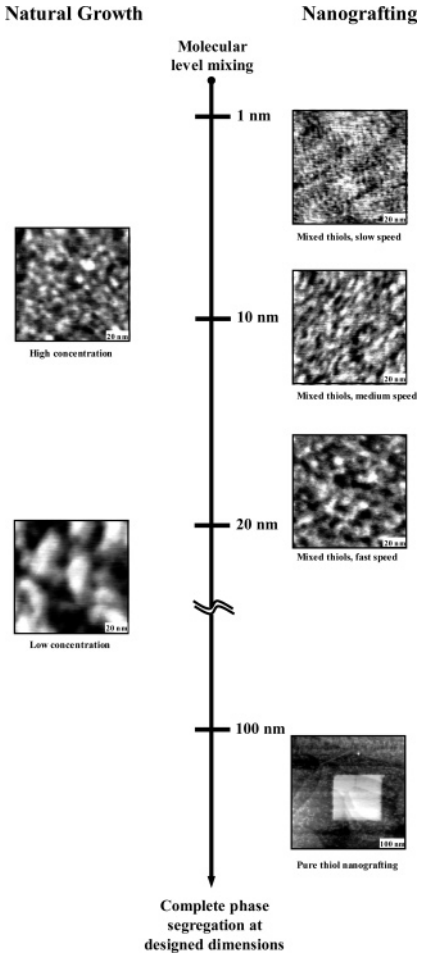

Figure 7. Schematic diagram summarizing the capability of nanografting to regulate local thiol domains, from molecular level mixing to nanometer level domains to structures with designed geometry and dimension.

difference is that the influence of solution concentration is less pronounced in nanografting in comparison to that in natural self-assembly. The C_{18} domain size increase in nanografting ranges from 2.5 to 5.9 and 8.1 nm for the three (0.2, 0.02, and 0.002 mM) concentrations, respectively. The quantitative difference between nanografting and natural growth is due to the reaction pathways as discussed previously. This systematic investigation provides a means to fine-tune the size of local domains formed in nanografting using self-assembly reaction conditions, i.e., the overall concentration. Analogous behavior is expected with the variation of the ratio of adsorbate species, functionality, and chain length, all of which provide additional means for the further refinement of the lateral heterogeneity in mixed SAMs formed during nanografting.

From the perspective of nanofabrication, nanografting allows regulation of lateral heterogeneity from molecular level mixing, to nanometer-sized local domains, to structures with designed geometry and dimensions (nanografting in single-component thiol solutions). Figure 7 summarizes the regulation of lateral domain segregation as measured by the increase of domain size. In natural self-assembly (left column), the interplay of thermodynamics and kinetics may be varied using surface reaction conditions, e.g. lowering concentration and increasing reaction time favors the thermodynamic product—more complete segregation. For alkanethiols, we were able to attain local domain sizes ranging from 5 to 50 nm. In nanografting under the same mixed solution as natural self-assembly, the regulation of lateral heterogeneity is obtained by varying the shaving speed. The resulting SAMs exhibit local structures ranging from nearly molecular level mixing, to several nanometers, to the limit of natural growth (such as 50 nm). The protocols are simple, and refined adjustment is attainable as speed in AFM can be varied in fine steps. One can always produce structures with designed geometry and size using single-component thiols with the required functionality.[31−33]

Conclusions

A new nanoengineering approach to regulate the lateral heterogeneity of mixed SAMs is reported using AFM (this article) and Monte Carlo simulations.[40] Despite the complexity of surface reactions of thiol mixtures with gold, the reaction pathway is known to include a lying-down phase, followed by a lying-down to standing-up phase transition. Many investigations (by us and many other researchers) of natural self-assembly have revealed the domain formation in mixed SAMs. The local structure reflects the interplay between kinetics and thermodynamics of the adsorption, and therefore depends on reaction conditions such as concentration, component ratio, reaction time, and interaction energy among thiols (chain-length and functionality). In nanografting, thiol attachment to gold can follow an unconstrained growth pathway or a spatially confined self-assembly pathway. The choice of the reaction pathways at given locations depends on the transient local environment, i.e. spatial constraint during the nanofabrication process. In actual nanografting, we believe that the two pathways are followed depending on the location and transient spatial confinement. Therefore, the lateral heterogeneity of the SAM in nanografting can be regulated by varying the shaving speed to adjust the local environment, and thus the reaction pathway. For nanografting in a given mixed thiol solution, we are able to produce local structures ranging from molecular level mixing to component segregation defined by the limit of natural self-assembly. Larger domains with designed geometry and size may be attained by nanografting in a selected single-component thiol solution. This systematic investigation further elucidates the reaction mechanism of the nanografting process, thus providing a new and simple means to regulate the local structure of mixed SAMs.

Acknowledgment. The new model for self-assembly during nanografting shown in Figure 5 was constructed in conjunction with Drs. Schatz and Ryu at Northwestern University (see also the companion paper). We thank Drs. Maozi Liu and Guohua Yang, and Ms. Shannon Leigh at University of California, Davis, for technical assistance and helpful discussions. This work was supported by the University of California, Davis, UC Discovery Grant in conjunction with Novartis Corp., and National Science Foundation under Grants NIRT CHE 0210807 and CHE 0244830. J.J.Y. acknowledges Tyco Electronics Foundation for a Graduate Fellowship in Functional Materials.

Supporting Information Available: Detailed derivation of the surface concentration of binary SAMs as predicted by thermodynamics; a specific example is a binary C_{18}/C_{10} SAM formed in a mixed C_{18}/C_{10} thiol solution with a molar ratio of 3:5. This material is available free of charge via the Internet at http://pubs.acs.org.

JA0631403